Ligand field-actuated redox-activity of acetylacetonate

Morten Gotthold Vinum,[1,‡] Laura Voigt,[1,‡] Steen H. Hansen,[1] Colby Bell,[2] Kensha M. Clark,[2] René Wugt Larsen,[1] and Kasper S. Pedersen[1,]*

[1] Department of Chemistry, Technical University of Denmark, DK-2800 Kgs. Lyngby, Denmark
[2] Department of Chemistry, The University of Memphis, Memphis, TN, USA

[‡] Equally contributing authors
** Correspondence to K.S.P. (kastp@kemi.dtu.dk)*

Chemical Science

Synthesis

All reactions and manipulations were carried out under strictly anaerobic conditions in an inert Ar atmosphere using an InertLab glovebox operating with < 0.5 ppm O_2 and H_2O. Reagents were used as received. Dry and air-free solvents were supplied by a Puresolv MD 7 solvent purifications system. acacH = 2,4-pentanedione; py = pyridine; DMAP = 4-(dimethylamino)pyridine; CF_3py = 4-(trifluoromethyl)pyridine.

*Synthesis of $Cr(acac)_2$ (**1**)*

In a beaker, $CrCl_2$ (367 mg, 3.0 mmol) was suspended in dry THF (20 mL) and Li(acac) (630 mg, 5.95 mmol) was added under stirring. The mixture slowly turned dark and the reaction proceeded to completion over a 24-hour period. An orange single-crystalline precipitate of the desired compound separated out and was filtered off, washed with diethyl ether (2 × 10 mL) and dried on a glass frit. Yield: 524 mg (70% based on Cr). Crystals suitable for X-ray analysis could be isolated directly from the product. Elemental analysis calculated (found) for $C_{10}H_{14}CrO_4$ (%): C: 48.00 (47.68), H: 5.64 (6.12).

*Synthesis of $Cr(acac)_2(CF_3py)_2$ (**2**)*

To a suspension of **1** (100 mg, 0.4 mmol) in toluene (2 mL) was added 4-trifluoromethylpyridine (0.20 mL, 1.7 mmol). The solution was stirred for 5 min during which the solution changed color to black. A precipitate of **2** started forming within minutes. The mixture was allowed to stand for 1 hour to ensure complete precipitation. Yield: 150 mg (69% based on **1**). Crystals suitable for X-ray analysis could be isolated directly from the product. Elemental analysis calculated (found) for $C_{22}H_{22}N_2O_4F_6Cr$ (%): C: 48.54 (47.11), H: 4.07 (4.13), N: 5.15 (4.82).

*Synthesis of $Cr(acac)_2(py)_2$ (**3**)*

To a suspension of **1** (108 mg, 0.43 mmol) in acetonitrile (2 mL) was added pyridine (2 mL). The solution was stirred for 2 min during which the solution changed color to a very dark green. The mixture was left at room temperature for 24 hours to ensure complete precipitation of **3**. Yield: 120 mg (68% based on **1**). Crystals suitable for X-ray analysis could be isolated directly from the product. Elemental analysis calculated (found) for $C_{20}H_{24}CrN_2O_4$ (%): C: 58.82 (58.73), H: 5.92 (6.02), N: 6.86 (6.78).

*Synthesis of $Cr(acac)_2(DMAP)_2$ (**4**)*

To a suspension of **1** (135 mg, 0.54 mmol) in acetonitrile (5 mL) was added a solution of 4-(dimethylamino)pyridine (205 mg, 1.68 mmol) dissolved in acetonitrile (2.5 mL). The solution was stirred for 10 min during which it changed color to black and the precipitation of **4** started. The solution was allowed to stand for 24 hours to ensure complete crystallization. Yield: 195 mg (73% based on

1). Crystals suitable for X-ray analysis could be isolated directly from the product. Elemental analysis calculated (found) for $C_{24}H_{34}CrN_4O_4$ (%): C: 58.29 (58.16), H: 6.93 (7.02), N: 11.33 (11.09).

Spectroscopy

Solution ultraviolet-visible range absorption spectra of **1** in various solvents were acquired using a Cary 5 spectrophotometer and are compiled in Fig. S1. Spectra to 2300 nm were collected on a PerkinElmer Lambda 1050 UV/VIS/NIR Spectrometer. The spectra have all been corrected for instrumental and solvent background. The attenuated-total-reflectance (ATR) NIR spectra of solid, polycrystalline samples of **1**–**4**, presented in the main text (Fig. 4), were collected using a Bruker VERTEX80v Fourier Transform vacuum spectrometer employing a single-reflection diamond ATR module. The apparatus was configured with a CaF_2 beam splitter, a liquid nitrogen cooled InSb detector and a NIR tungsten radiation source. The collected ATR spectra of 4 cm^{-1} resolution have been corrected for residual water vapor absorption and the resulting spectra have been corrected for minor baseline drifts. Subsequently, extended ATR corrections were applied to account for the wavelength-dependent penetration depth of the NIR probe beam. The mid-infrared attenuated-total-reflectance spectra in the fingerprint region were collected by a Bruker VERTEX80v Fourier transform vacuum spectrometer employing a single-reflection diamond ATR accessory. The apparatus was configured with a KBr beam splitter, a liquid-nitrogen-cooled HgCdTe detector, and a thermal globar radiation source. The spectra were subtracted for residual water vapor absorption, corrected for small baseline drifts and extended ATR corrections were applied to account for the wavelength-dependent penetration depth of the probe beam. NMR spectra were collected on 400 MHz JEOL cryoprobe NMR spectrometer in dry, degassed dichloromethane-d_2 at 298 K. ^{1}H-NMR spectra were referenced to tetramethylsilane using the residual proteo impurities of the solvent.

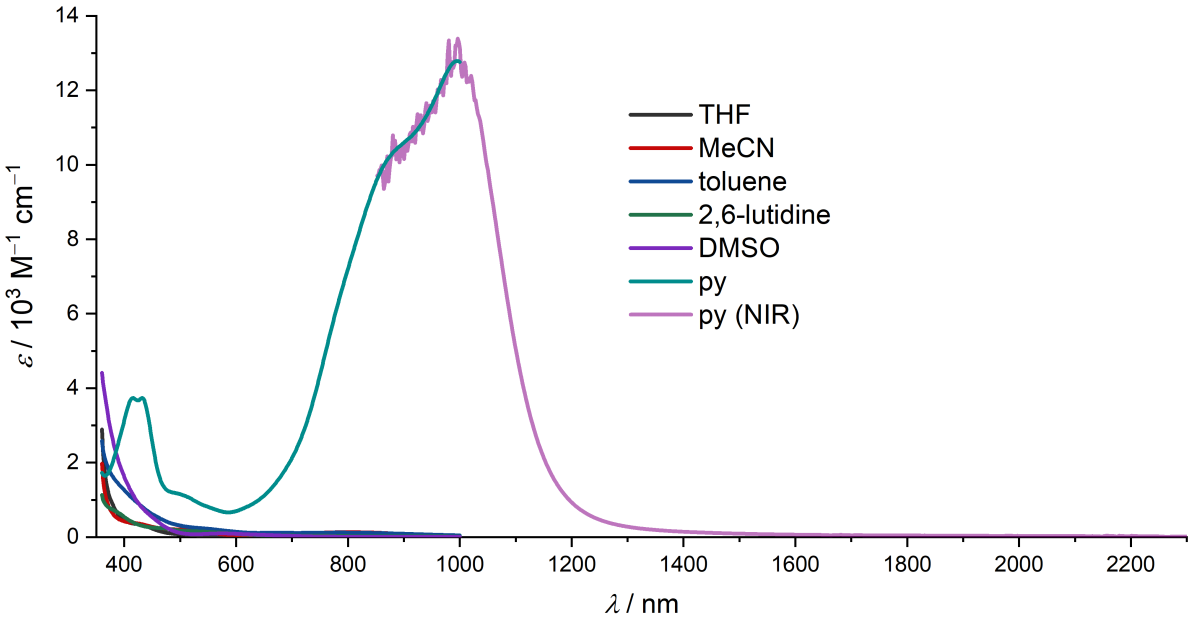

Figure S1. Solution UV-vis spectra of **1** dissolved in different, indicated solvents. The concentration of **1** in each solvent was: THF: 1.30×10^{-4} M, MeCN: 1.33×10^{-4} M, toluene: 1.34×10^{-4} M, 2,6-lutidine: 1.37×10^{-4} M, DMSO: 1.37×10^{-4} M, py: 1.29×10^{-4} M.

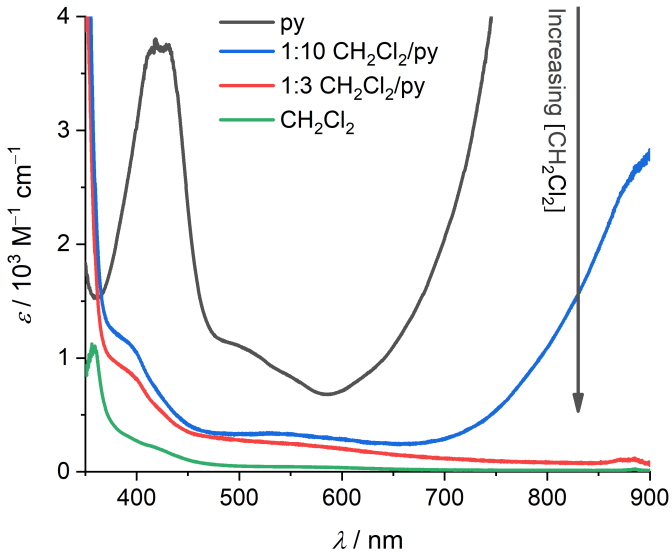

Figure S2. Solution UV-vis spectra of **3** in neat pyridine (py, black trace; compare to turquoise trace of Fig. S1) and CH_2Cl_2 (green traces) and mixtures thereof (blue and red traces).

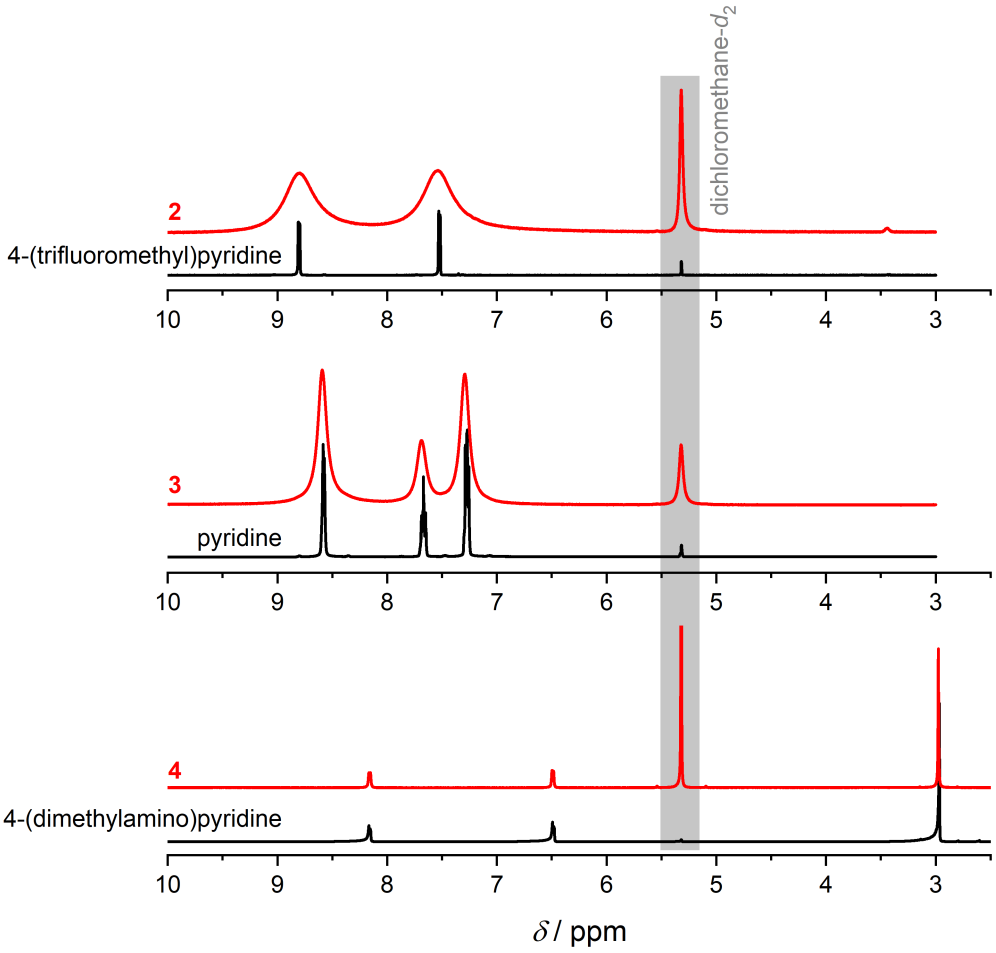

Figure S3. ^{1}H-NMR spectra of **2**–**4** acquired at room temperature in CD_2Cl_2. The spectra of the free ligands are shown for comparison.

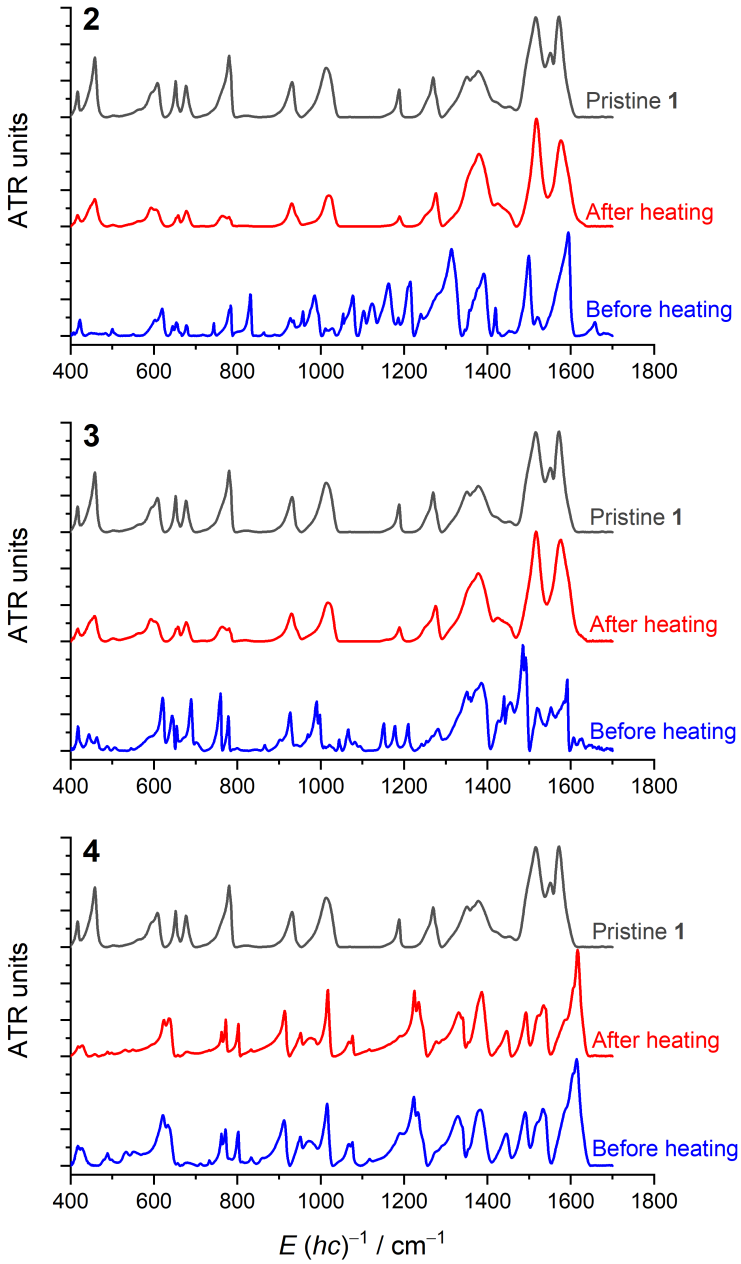

Figure S4. ATR-mid-IR spectra of **2**–**4** before and after heating to 400 K (1 K min^{-1}). The spectra for pristine **1** is shown for comparison.

Crystallography

Single crystals of **1**–**4** were sealed under a dry argon atmosphere using polybutene oil (Aldrich, >90%) before being exposed to ambient conditions. With a nylon loop, suitable crystals were selected under a microscope and mounted on a SuperNova Dual Source CCD-diffractometer. The crystal was kept at a constant temperature during data collection. Using Olex2,[1] the structure was solved using Charge Flipping using the olex.solve.structure solution program of Olex2 and refined by Least Squares using version 2014/7 of ShelXL.[2] All non-hydrogen atoms were refined anisotropically. Hydrogen atom positions were calculated geometrically and refined using the riding model.

The PXRD patterns of **1**-**4** were measured in sealed tape pockets (free of sharp Bragg-like peaks) in transmission with a Huber G670 powder diffractometer using Cu Kα1 (λ = 1.5406 Å, quartz monochromator) radiation. Samples measured after a PPMS experiment were first introduced back into an inert atmosphere, before being freed from the measurement capsule and subsequently sealed in a tape pocket.

Table 1. Crystallographic information and refinement parameters for **1–4**.

Compound	**1**	**2**	**3**	**4**
CCDC number	1974983	1974982	1974980	1974981
Empirical formula	$C_{10}H_{14}CrO_4$	$C_{22}H_{22}N_2O_4F_6Cr$	$C_{20}H_{24}CrN_2O_4$	$C_{24}H_{34}CrN_4O_4$
Formula weight / g mol^{-1}	250.21	544.41	408.41	494.55
Temperature / K	120.00	120	120	120.00
Crystal system	monoclinic	monoclinic	monoclinic	triclinic
Space group	$P2_1/n$	$P2_1/c$	$P2_1/n$	$P\bar{1}$
a / Å	10.2476(13)	9.9399(10)	9.8861(8)	7.9894(7)
b / Å	4.7011(6)	9.5252(9)	7.5065(8)	8.5405(8)
c / Å	11.3501(15)	12.1430(10)	12.9438(10)	9.4779(9)
α / °	90	90	90	103.054(8)
β / °	92.163(12)	94.290(8)	94.152(7)	101.710(8)
γ / °	90	90	90	92.188(7)
Volume / Å^3	546.40(12)	1146.47(18)	958.04(14)	614.49(10)
Z	2	2	2	1
ρ_{calc} / g cm^{-3}	1.521	1.577	1.416	1.336
μ / mm^{-1}	1.037	0.580	0.625	0.502
F(000)	260.0	556.0	428.0	262.0
Radiation	Mo Kα (λ = 0.71073)	Mo Kα (λ = 0.71073)	Mo Kα (λ = 0.71073)	Mo Kα (λ = 0.71073)
θ range for data collection / °	7.2–52.7	6.7–54.2	6.3–54.2	6.9–52.7
Index ranges	$-12 \le h \le 12$	$-9 \le h \le 12$	$-10 \le h \le 12$	$-9 \le h \le 8$
	$-5 \le k \le 4$	$-12 \le k \le 12$	$-9 \le k \le 6$	$-10 \le k \le 8$
	$-10 \le l \le 14$	$-15 \le l \le 15$	$-14 \le l \le 16$	$-11 \le l \le 11$
Reflections collected	2302	5379	4889	5094
Independent reflections	1114 [R_{int} = 0.0636]	2477 [R_{int} = 0.0492]	2086 [R_{int} = 0.0514]	2494 [R_{int} = 0.0526]
Data/restraints/parameters	1114/0/72	2477/0/162	2086/0/126	2494/0/155
Goodness-of-fit on F^2	1.073	1.046	1.034	1.091
Final R_1 index [$F^2 \ge 2\sigma(F^2)$]	0.062	0.063	0.0488,	0.060
Final wR_2 index [F^2]	0.095	0.126	0.0895	0.105
Largest diff. peak/hole / e Å^{-3}	0.54/–0.51	0.74/–0.55	0.45/–0.47	0.35/–0.39

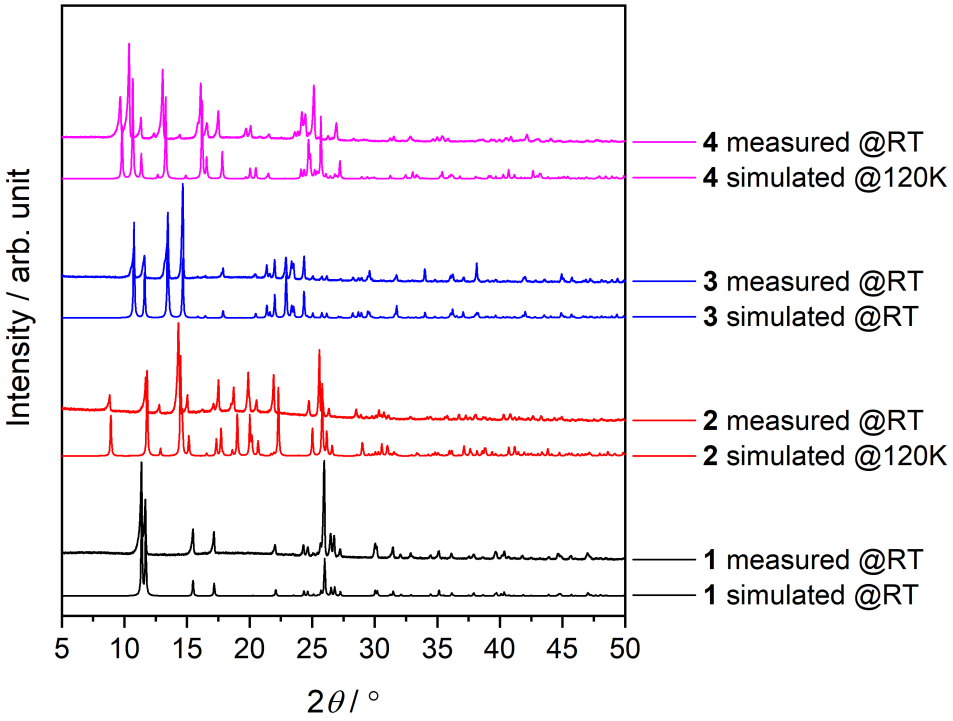

Figure S5. Normalized room-temperature (RT) powder X-ray diffractograms of **1**–**4** and the simulated powder diffractograms obtained from the single-crystal X-ray structures at the indicated temperatures.

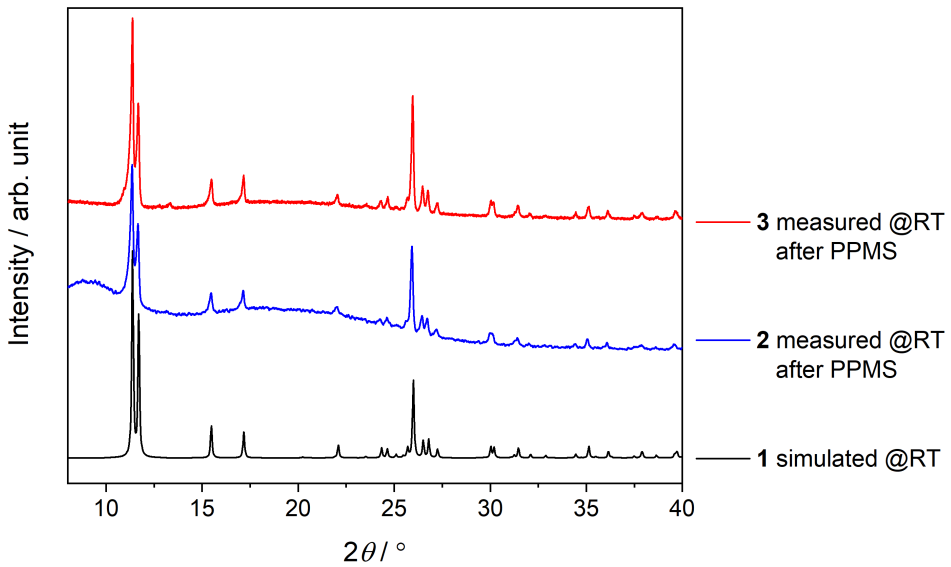

Figure S6. Normalized room-temperature (RT) powder X-ray diffractograms of **2** and **3** after the magnetization experiments shown in Fig. 3 of the main text, and the simulated powder diffractogram of **1**.

Electrochemical measurements

The electrochemical experiments were performed on a Gamry Reference 600+ Potentiostat/Galvanostat/ZRA (Gamry Instruments, Warminster, PA, USA) equipped with a 3.0 mm glassy carbon working electrode, a platinum wire auxiliary electrode, and a silver wire reference electrode. All experiments were performed at room temperature in an N_2-filled glovebox. Sample concentrations were 1.0 mM in pyridine with 0.10 M NBu_4PF_6 as the supporting electrolyte. All potentials are referenced to $Cp^*_2Fe^{0/+}$, using Cp^*_2Fe as an internal standard. The typical solvent system window with our configuration was +0.5 V for the oxidation limit and –2.25 V for the reduction limit (vs $Cp^*_2Fe^{0/+}$). Cp_2Fe (Strem) was purified according to the previously reported literature procedures. [3] Pyridine (Fisher) was dried over calcium hydride and distilled freshly. Tetrabutylammonium hexafluorophosphate (Acros) was recrystallized three times from ethanol and dried under a dynamic vacuum.[4]

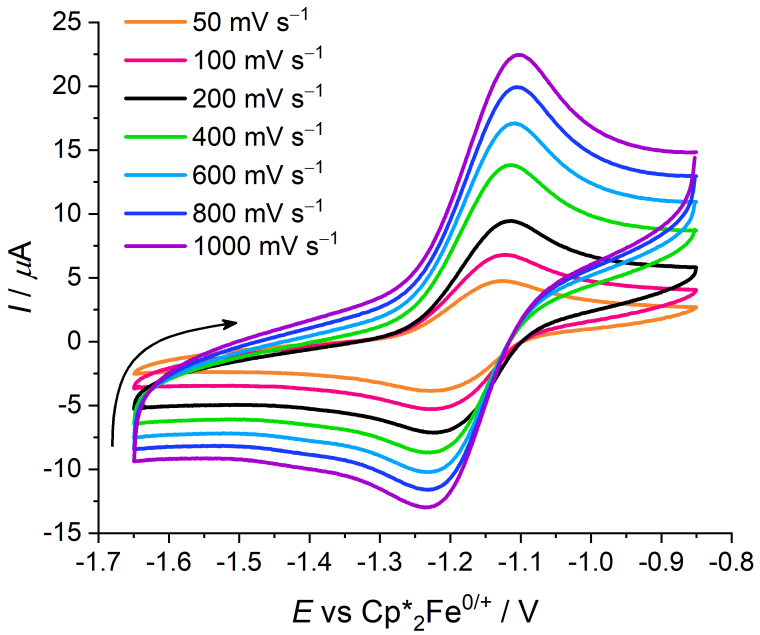

Figure S7. Cyclic voltammograms of **3** (1.0 mM) in neat pyridine at selected scan rates. NBu_4PF_6 (0.1 M) was used as supporting electrolyte.

Magnetic measurements

Direct current magnetization measurements were performed using the VSM options on a QuantumDesign Dynacool PPMS in the temperature range from 1.7 K to 400 K and in magnetic fields up to $\mu_0 H$ = ±9 T. The polycrystalline samples were loaded, immobilized and sealed in standard QuantumDesign powder capsules inside an argon-filled glovebox. The accurate sample masses were determined using a Mettler-Toledo WXTS3DU microbalance. The magnetization data were corrected for the intrinsic diamagnetism of both the sample and the sample capsule.

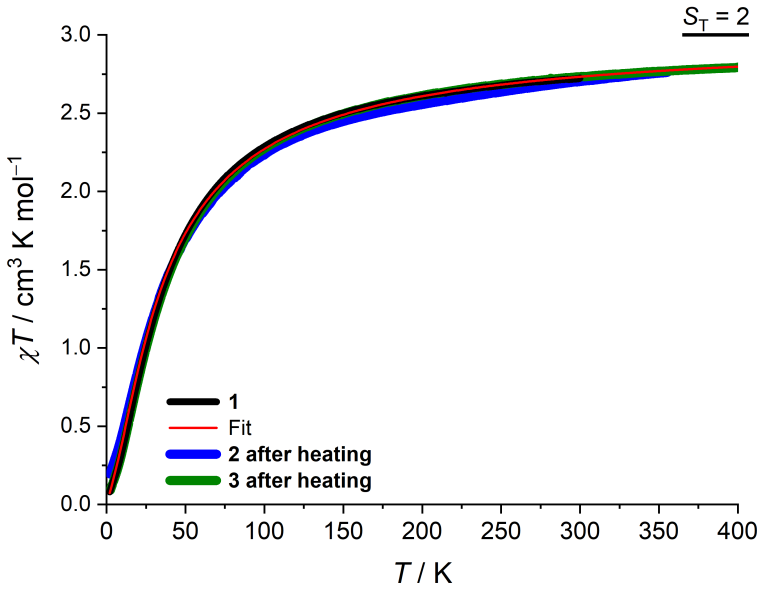

Figure S8. Cooling χT ($\mu_0 H$ = 1 T) data for the heated samples of **2** and **3** plotted together with the data for pristine **1** and the Fisher-model fit as described in the main text.

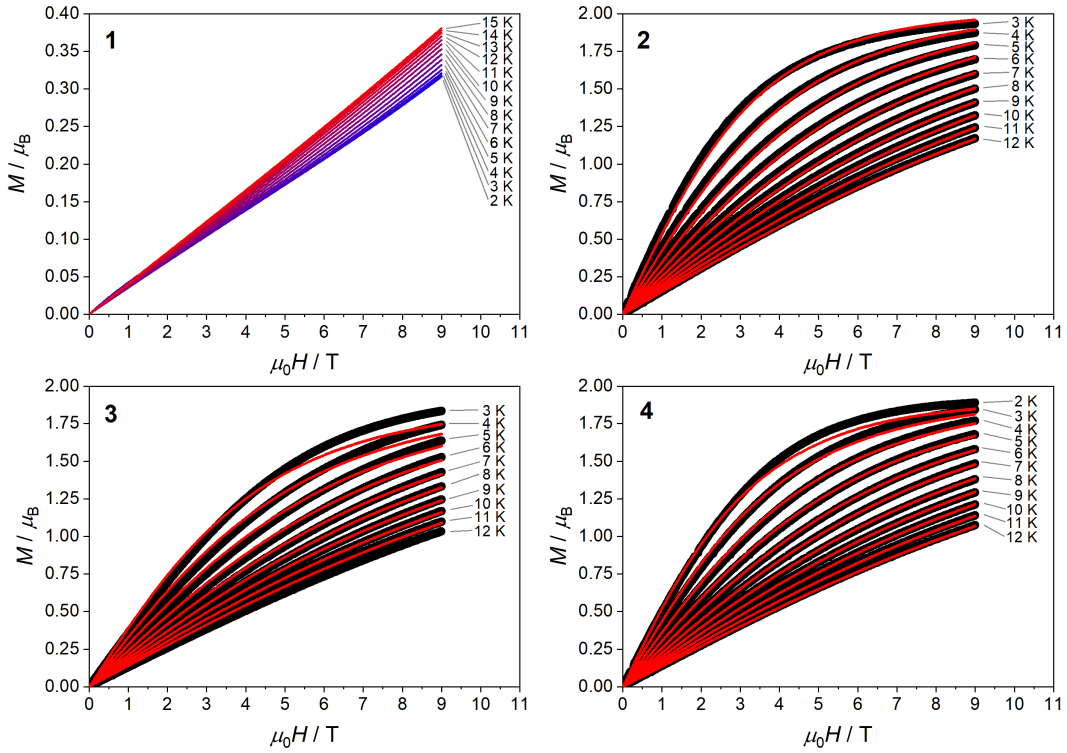

Figure S9. *M* vs $\mu_0 H$ data for polycrystalline **1**–**4** obtained at selected low temperatures. Solid red lines (**2**–**4**) are best fits using the Hamiltonian mentioned in the main text. The best fits revealed **2**: g = 2.0, $D_{S_T = 1}/hc$ = +2.2 cm^{-1}; **3**: g = 1.9, $D_{S_T = 1}/hc$ = +4.2 cm^{-1}; **4**: g = 1.9, $D_{S_T = 1}/hc$ = +3.7 cm^{-1}.

Thermogravimetry-mass spectrometry

Thermogravimetric analysis was performed using a Perkin-Elmer STA 6000 instrument, coupled with a Hiden HPR 20 QIC mass spectrometer. A heating rate of 1 K min^{-1} was applied and a protective argon flow of 30 mL min^{-1} was maintained throughout the experiments. The mass spectrometer was set up accordingly, to detect fragment mass units (*m*/*z*) 51, 69, and 75 for **2** and 52, and 79 for **3**. The mass spectrum of pristine 4-(trifluoromethyl)pyridine is shown in Fig. S11 and the mass spectrum of pyridine can be assessed from the National Institute of Standards and Technology.[5] The sample crucible was a corundum (Al_2O_3) container fitted with a separate lid, perforated in the center, to allow release of pressure build-up from any desorbed species.

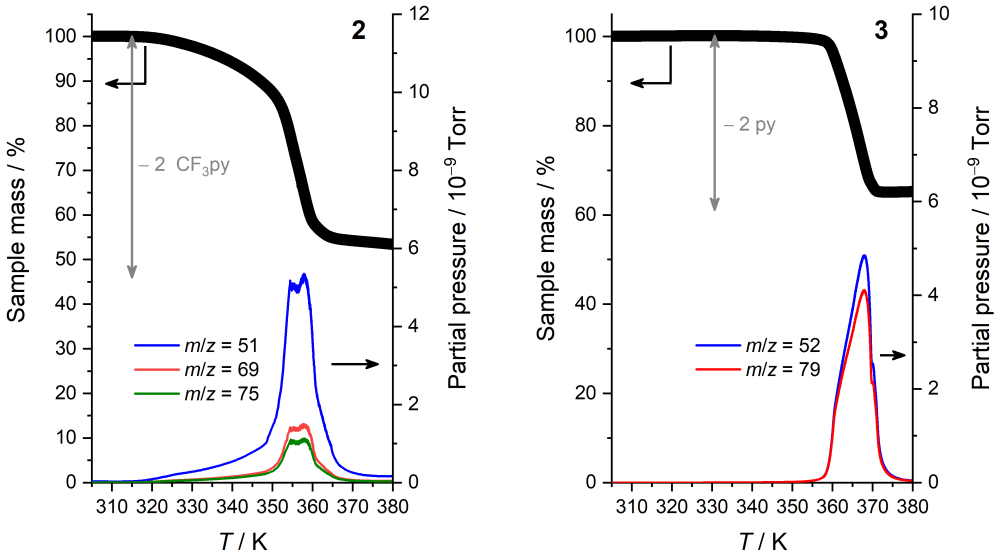

Figure S10. TGA-MS data for **2** (left) and **3** (right) obtained with a 1 K min^{-1} heating rate. Gray arrows indicate the calculated weight losses for quantitative removal of the axial ligands.

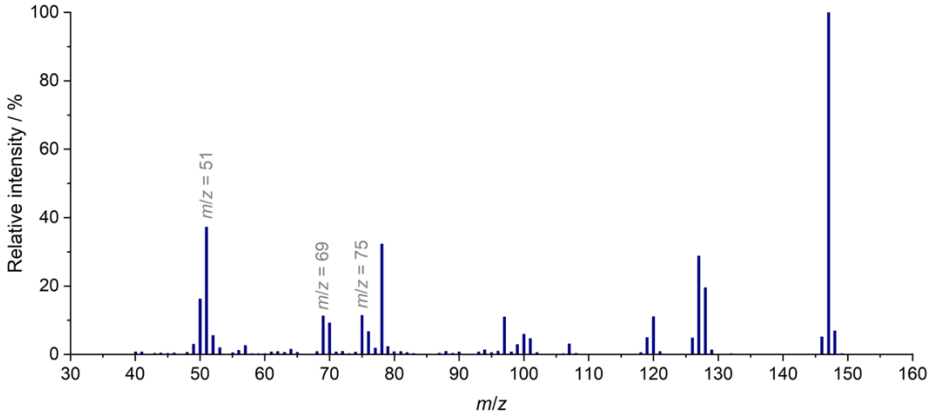

Figure S11. Positive-ion mass spectrum of 4-(trifluoromethyl)pyridine obtained on a GC-2010 MS-QP2010S.

Computational results

DFT calculations were performed using the ORCA program suite,[6] employing scalar relativistic effects through the 0th-order regular approximation (ZORA).[7] The experimentally determined atomic coordinates of **1** and **2** were used as input without any subsequent geometry optimization. For all calculations, the TPSSh functional[8] was combined with the scalar-relativistically recontracted (SARC) version of the triple-ζ def2-TZVP(-f) basis set[9] together with the corresponding auxiliary basis. For both systems a high-spin (HS) $S = 2$ calculation and a $S_1 = 3/2$ - $S_2 = 1/2$ broken symmetry calculation (BS(3,1)) were performed. The energy difference between the HS and BS states were employed to evaluate the exchange coupling constant, J, as defined by Yamaguchi.[10] Spin density plots and Kohn-Sham frontier orbital plots were rendered using the VMD[11] and Gabedit[12] programs, respectively.

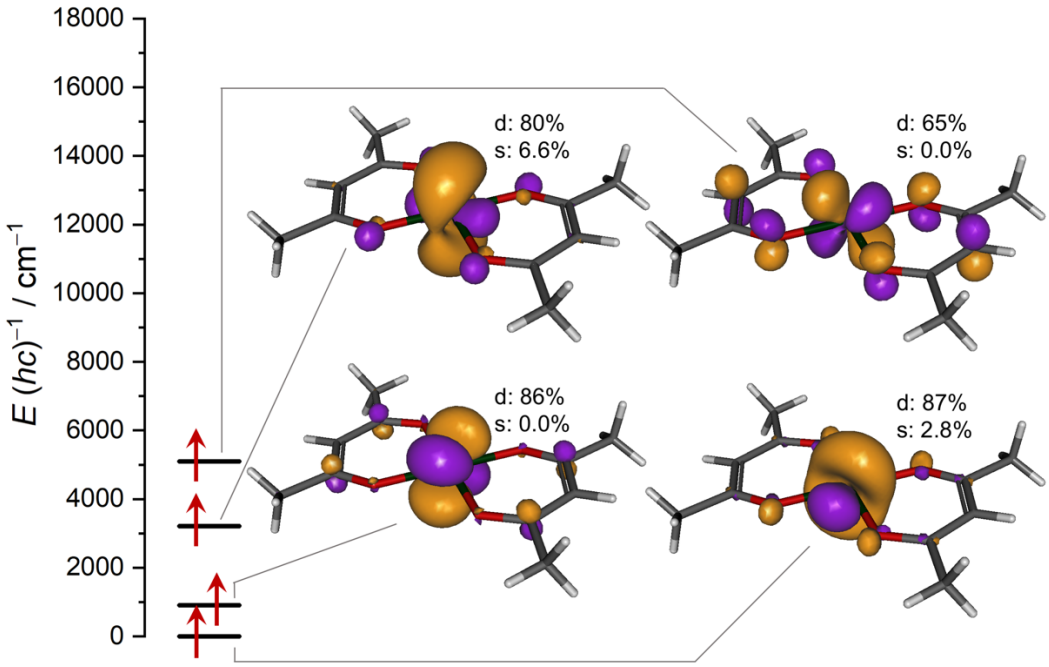

Figure S12. Qualitative frontier Kohn-Sham SOMO energy level diagram for **1** with indicated calculated relative energies and percental contribution of Cr atomic orbitals to the MOs.

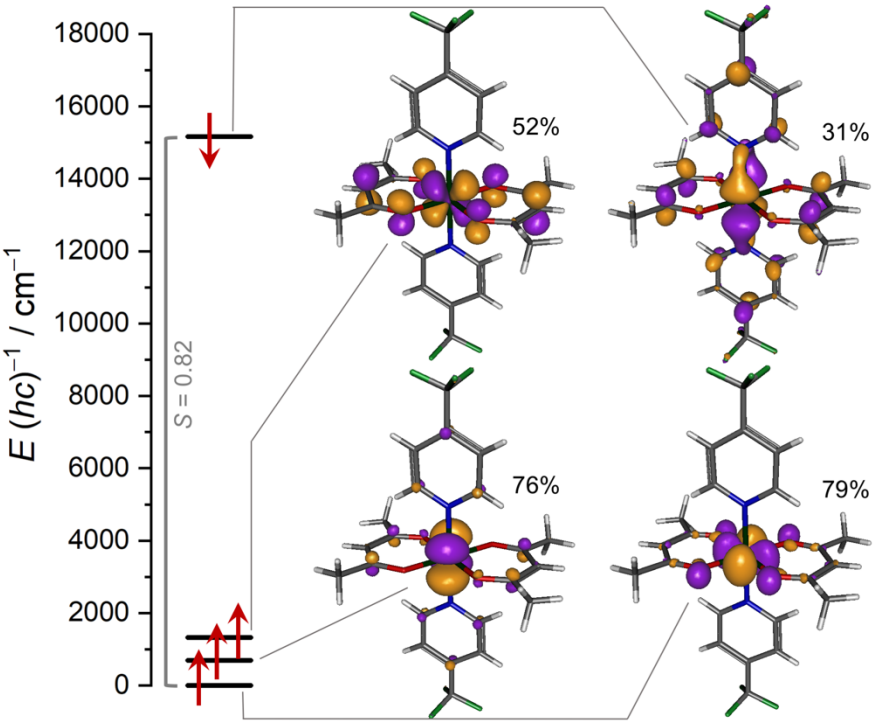

Figure S13. Qualitative frontier Kohn-Sham spin-orbital energy level diagram for **2** with indicated calculated relative energies, percental contribution of Cr atomic orbitals to the MOs, and overlaps between corresponding orbitals.

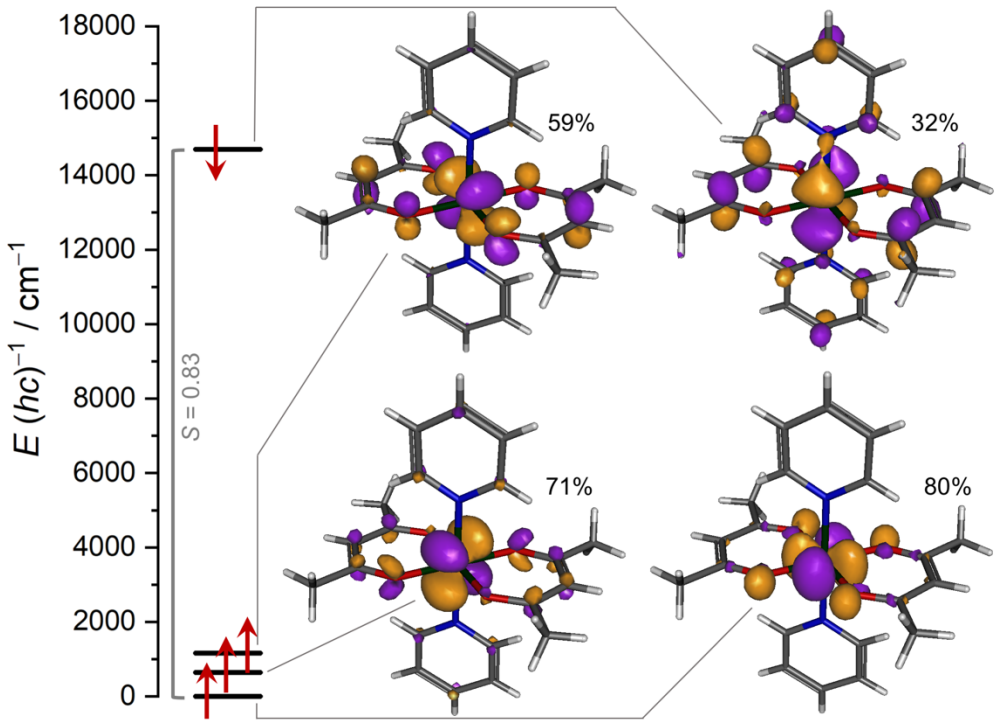

Figure S14. Qualitative frontier Kohn-Sham spin-orbital energy level diagram for **3** with indicated calculated relative energies, percental contribution of Cr atomic orbitals to the MOs, and overlaps between corresponding orbitals.

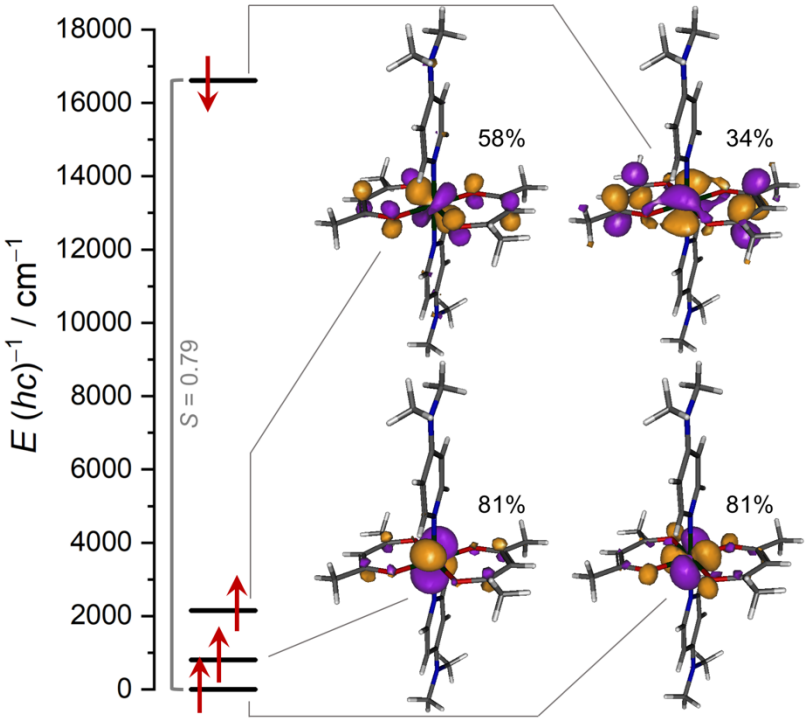

Figure S15. Qualitative frontier Kohn-Sham spin-orbital energy level diagram for **4** with indicated calculated relative energies, percental contribution of Cr atomic orbitals to the MOs, and overlaps between corresponding orbitals.

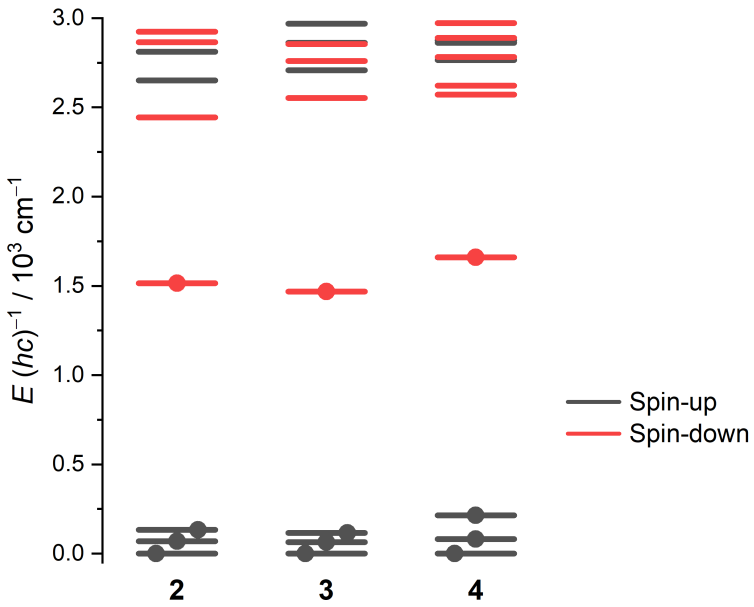

Figure S16. Kohn-Sham spin-orbital energy level diagram for **2**–**4**. Occupied orbitals are indicated with a dot.

References

[1] H. Dolomanov, O.V., Bourhis, L.J., Gildea, R.J, Howard, J.A.K. & Puschmann, *J. Appl. Cryst.*, 2009, **42**, 339.

[2] G. M. Sheldrick, *Acta Cryst.*, **A71**, 3–8.

[3] a) R. B. King, M. B. Bisnette, *J. Organometal. Chem.* **1967**, *8*, 287; b) A. Zahl, R. van Eldik, M. Matsumoto, T.W. Swaddle, *Inorg. Chem*. **2003**, *42*, 3718; c) J. Coddington, S. Wherland, *Inorg. Chim. Acta* **1996**, *242*, 159.

[4] R. L. Bedard, L.F. Dahl, *J. Am. Chem. Soc.* **1986**, *108*, 5933.

[5] NIST Mass Spectrometry Data Center, William E. Wallace, director, "Mass Spectra" in NIST Chemistry WebBook, NIST Standard Reference Database Number 69, Eds. P.J. Linstrom and W.G. Mallard, National Institute of Standards and Technology, Gaithersburg MD, 20899, https://doi.org/10.18434/T4D303, (retrieved June 29, 2020).

[6] F. Neese, *WIREs Comput. Mol. Sci.* **2018**, *8*, e1327

[7] a) E. van Lenthe, E. J. Baerends, J. G. Snijders, *J. Chem. Phys.* **1993**, *99*, 4597; b) C. J. van Wüllen, *J. Chem. Phys.* **1998**, *109*, 392.

[8] V. N. Staroverov, G. E. Scuseria, J. Tao, J. P. Perdew, *J. Chem. Phys.* **2003**, *119*, 12129.

[9] a) F. Weigend, R. Ahlrichs, *Phys. Chem. Chem. Phys.* **2005**, *7*, 3297; b) D. A. Pantazis, X.-Y. Chen, C. R. Landis, F. Neese, *J. Chem. Theory Comput*. **2008**, *4*, 908.

[10] a) K. Yamaguchi, Y. Takahara, T. Fueno, in *Applied Quantum Chemistry*; V. H. Smith, H. F. Schaefer, K. Morokuma, Eds.; D. Reidel: Boston, **1986**; p. 155; b) S. Yamanaka, T. Kawakami, H. Nagao, K. Yamaguchi, *Chem. Phys. Lett.* **1994**, *231*, 25.

[11] a) W. Humphrey, A. Dalke, K. Schulten, *J. Molec. Graphics* **1996**, 14, 33; b) Website: http://www.ks.uiuc.eu/Researcg/vmd

[12] a) A.-R. Allouche, *J. Comput. Chem*. **2010**, *32*, 174; b) Website: https://sites.google.com/site/allouchear/Home/gabedit